



Biosorption of methylene blue from aqueous solution by natural *Osmanthus fragrans* powder

Bo Chai*, Xianzhong Cheng, Zhandong Ren, Yuchan Zhu

School of Chemical and Environmental Engineering, Wuhan Polytechnic University, Wuhan 430023, P.R. China,
Tel. +86 27 8394 3956; email: willycb@163.com

Received 18 March 2015; Accepted 10 September 2015

ABSTRACT

The potential of *Osmanthus fragrans* powder as a natural biosorbent was investigated for the removal of methylene blue (MB) from aqueous solution. The effects of various experimental conditions including contact time, adsorbent dose, initial MB concentration, solution pH, salt ionic strength, and temperature on the adsorption properties of *O. fragrans* powder were discussed. The adsorption kinetic data were modeled using pseudo-first-order, pseudo-second-order, and intraparticle diffusion kinetics equations, indicating that the pseudo-second-order and intraparticle diffusion models could better describe the adsorption kinetics. Furthermore, adsorption equilibrium data were analyzed by Langmuir and Freundlich models, suggesting the Langmuir model presented a better correlation with the experimental data. The maximum adsorption capacities (q_m) of *O. fragrans* powder for MB obtained from the Langmuir model were 155.52, 165.02, and 172.71 mg g⁻¹ at different temperatures of 288.15, 298.15, and 308.15 K, respectively. Thermodynamic parameters such as standard free energy changes (ΔG°), standard enthalpy changes (ΔH°), and standard entropy changes (ΔS°) were also calculated. The results showed that the adsorption process was spontaneous and endothermic in nature. In addition, the possible adsorption mechanism of *O. fragrans* powder as adsorbent was proposed. The present study implies that *O. fragrans* powder were a promising candidate as novel biosorbents for the removal of MB from aqueous solution.

Keywords: Adsorption; Methylene blue; *Osmanthus fragrans* powder; Isotherm; Kinetics

1. Introduction

Dyes are widely used in the textile, paper, plastic, leather, food, and cosmetic industry to color products. The release of colored effluents from these industries may cause various environmental problems. For example, the presence of dyes in water can affect photosynthetic processes of aquatic plants to reduce oxygen levels in water, and in severe cases, resulting in the

suffocation of aquatic flora and fauna. Additionally, many of these dyes are carcinogenic, mutagenic, and toxic to human beings, microorganisms, and fish species. Hence, the removal of dyes from industrial effluents before discharging into the environment is extremely necessary [1,2].

Nowadays, various removal methods have been developed in the wastewater treatment, such as adsorption [1], membrane separation [3], coagulation [4], biological treatment [5], photocatalysis [6], and

*Corresponding author.

other processes. Among these methods, adsorption is the most widely used approach because of the ease of operation and low cost. As we all know, commercial activated carbon is a very effective adsorbent due to its high surface area, but a relatively high cost may limit the use of activated carbon. Recently, various low-cost adsorbents derived from agricultural wastes or natural materials have been explored intensively for removal of pollutants from aqueous solutions, such as sugarcane bagasse [7], *Lemna aquinoctialis* [8], papaya seeds [9,10], fruit peels [11–13], plant leaves [14–18], pine cone [19], hazelnut shell [20], grass waste [21], wood apple shell [22], silkworm exuviae [23], and so on. These biomaterial adsorbents have showed great potential for the treatment of dye wastewaters owing to very large quantities, ease of getting, and very low costs.

Osmanthus fragrans is a plant belonging to the *Oleaceae* family, which is planted from the southern China to southern Japan and Southeast Asia as far as Cambodia and Thailand. It is usually cultivated as an ornamental plant in Asia, Europe, North America, and elsewhere in the world for its delicious scent during flowering. The flowers of *O. fragrans* are often used as an additive for food, tea, and other beverages in China. Because of the abundance and cheapness of the flowers of *O. fragrans*, most of them are also directly discarded after withering. The disposal would cause the waste of resources, and then expanding the application scope of them is necessary. According to previous report [24], the flowers of *O. fragrans* contain a lot of alcohols, carboxylic acids, ionone, and esters, which make them adsorb dyes. Collection of the withered flowers of *O. fragrans* as adsorbents to remove dyes from wastewater is very meaningful. To our knowledge, there is no report on the use of the flowers of *O. fragrans* for the removal of dyes from aqueous solution. This work presents the possible use of the flowers of *O. fragrans* as a methylene blue (MB) dye adsorbent. The effects of solution pH, adsorbent dose, salt ionic strength, initial MB concentration, and temperature on the adsorption performances of *O. fragrans* flowers were investigated. In addition, the kinetics, adsorption isotherm, and thermodynamic parameters were explored to describe the experimental data.

2. Materials and methods

2.1. Preparation of adsorbent

Withered flowers of *O. fragrans* were collected from *O. fragrans* trees of the campus of Wuhan Polytechnic University in September. Then the flowers were continuously washed with tap water to remove dirt from

the surface. The washed flowers were dried at 80°C in oven for 24 h until constant weight. Dried flowers were ground into powder and then sieved through a 100-mesh sieve. The fine powder thus obtained was stored in a plastic bottle for further use. No other chemical or physical treatments were used prior to adsorption experiments.

2.2. Characterization of adsorbent

The surface morphology of *O. fragrans* powder was investigated with scanning electron microscopy (SEM) using Hitachi S-3000N operated at 15 kV. Fourier transform infrared spectra (FTIR) of samples were recorded on a Thermo Nicolet Avatar 360 spectrometer using conventional KBr pellets. The pH of the point of zero charge (pH_{pzc}) of the adsorbent was determined by the pH drift method described in previous reports [7,25,26]. The pH values of a solution of 0.01 M NaCl were adjusted from 2.0 to 10.0 by adding either HCl or NaOH solution. Nitrogen was bubbled through the solution at room temperature to remove dissolved carbon dioxide until the initial pH values (pH_i) stabilized. Then, 0.1 g of *O. fragrans* powder was, respectively, added into 50 mL of the above solution. The suspensions were shaken for 12 h and allowed to equilibrate for another 12 h. The final pH values (pH_f) of the supernatant liquids were recorded. The difference between the initial and final pH values ($\Delta\text{pH} = \text{pH}_f - \text{pH}_i$) was plotted against the pH_i . The point of intersection of the resulting curve at which $\Delta\text{pH} = 0$ gave pH_{pzc} .

2.3. Adsorption experiments

Adsorption isotherm experiments were performed by adding a specified amount of adsorbent samples (40 mg) to a series of conical flasks containing MB solutions (100 mL, 10–90 mg L⁻¹). The flasks were then sealed and placed in a thermostatic oscillator and shaken at 200 rpm for 160 min at 288.15, 298.15, and 308.15 K at the natural pH value (approximate 6.0). After centrifugation, the concentration of MB left in the supernatant solution was determined from the calibration curve prepared by measuring the absorbance of different predetermined concentrations of MB solutions at $\lambda_{\text{max}} = 664$ nm using a UV–vis spectrophotometer (TU-1810).

The equilibrium adsorption capacity q_e (mg g⁻¹) of the adsorbents was calculated from the following equation [27–29]:

$$q_e = \frac{(C_0 - C_e)V}{W} \quad (1)$$

where C_0 and C_e (mg L^{-1}) are the liquid-phase concentrations of MB at initial and equilibrium concentrations, respectively, V is the volume of the solution (L), and W is the mass of the adsorbent used (g).

To study the effect of adsorbent dose on the amount of dye adsorbed, different amounts of adsorbents (10, 20, 40, 60, 80, and 100 mg) were, respectively, added to 100 mL of MB solution with the initial concentration (70 mg L^{-1}) at the natural pH value and shaken at 298.15 K for 160 min. The dye removal percentage ($R\%$) was calculated as follows [14]:

$$R\% = \frac{(C_0 - C_e)}{C_0} \times 100\% \quad (2)$$

Batch kinetic experiments were carried out by mixing 40 mg of adsorbents to 100 mL of MB solution with a known initial concentration (50, 70, and 90 mg L^{-1}) at the natural pH value and shaken at 298.15 K for different time intervals. The concentration of MB left in the supernatant solution was analyzed as above. The amount of adsorption at time t , q_t (mg g^{-1}), was calculated by [27–29]:

$$q_t = \frac{(C_0 - C_t)V}{W} \quad (3)$$

where C_0 and C_t (mg L^{-1}) are the liquid phase concentrations of MB at the initial concentration and any time t , respectively, V is the volume of the solution (L), and W is the mass of the adsorbent used (g). For comparison, the commercial activated carbon (purchased from the Tianjin Bodi Chemical Reagent Co, Ltd) was chosen as adsorbent to evaluate the adsorption performance by adding 40 mg of activated carbon in 100 mL of 50 mg L^{-1} MB solution.

2.4. pH value and salt ionic strength effect

The effect of pH was performed by dispersion of 40 mg of adsorbents in 100 mL of 70 mg L^{-1} MB solution. The initial pH of the MB solution was adjusted from 2.0 to 10.0 using 0.1 mol L^{-1} HCl or 0.1 mol L^{-1} NaOH solution. The suspensions were shaken at 298.15 K for 160 min. The concentration of MB left in the supernatant solution was analyzed as above.

The effect of salt ionic strength on the adsorption properties was studied by adding different sodium salts (NaCl , Na_2SO_4 , CH_3COONa , NaNO_3 , and NaHCO_3) to 100 mL of 70 mg L^{-1} MB solution with the Na^+ ionic concentration ranging from 0 to 0.5 mol L^{-1} . The suspensions were shaken at 298.15 K for 160 min. The concentration of MB left in the supernatant solution was analyzed as above.

2.5. Different dye adsorption performance

Five types of organic dyes such as MB, Fuchsin basic (FB), Rhodamine B (RhB), Orange II (OII), and Malachite green (MG) were selected as study models to evaluate, respectively, the adsorption performances with 40 mg of adsorbents in 100 mL of 50 mg L^{-1} solution. The concentration of MB, FB, RhB, OII, and MG left in the supernatant solution was analyzed at $\lambda_{\text{max}} = 664, 542, 554, 485, \text{ and } 618 \text{ nm}$ using a UV-vis spectrophotometer, respectively.

3. Results and discussion

3.1. Characterization of adsorbent

Fig. 1 shows the SEM image of *O. fragrans* powder. It is clear that the *O. fragrans* powder have a rough surface with large amounts of pleats, which lead to the formation of numerous pores and cavities. This indicates that there is a good possibility for MB dye to be trapped and adsorbed onto the surface of *O. fragrans* powder [21]. The FTIR is an important technique to determinate characteristic functional groups, which make the adsorption behavior possible. Fig. 2 depicts the FTIR spectra of *O. fragrans* powder before and after MB adsorption. As shown in Fig. 2(a), the broad peak at about 3420 cm^{-1} corresponds to the stretching vibration mode of the hydroxyl group on the surface of *O. fragrans* powder. The peaks at 2935 and 2856 cm^{-1} are attributed to the stretching vibration of $-\text{CH}_3$ and $-\text{CH}_2$, respectively [14]. The strong band at 1630 cm^{-1} is characteristic of the stretching vibration of $\text{C}=\text{O}$ from carboxylic acid with intermolecular hydrogen bonding [14]. The peak at 1385 cm^{-1} is related to the bending vibration of $-\text{CH}_3$

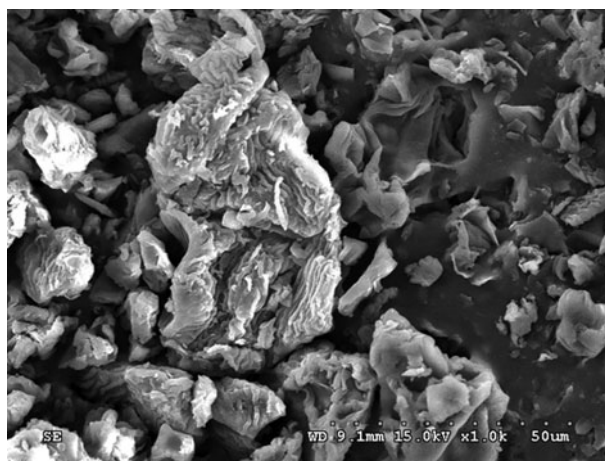


Fig. 1. SEM image of *O. fragrans* powder.

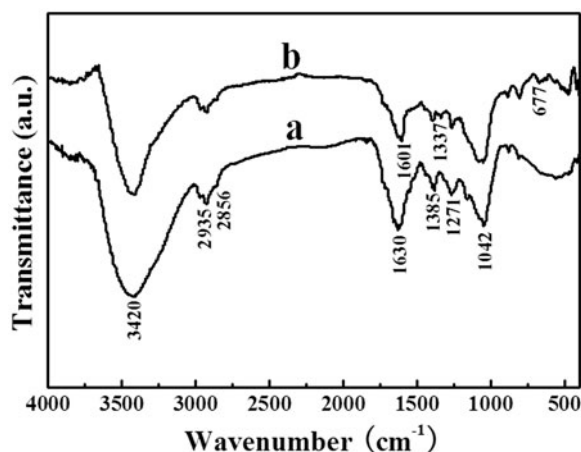


Fig. 2. FTIR spectra of *O. fragrans* powder before (a) and after (b) adsorption of MB.

and $-\text{CH}_2$. The peak at $1,271\text{ cm}^{-1}$ belongs to epoxy C–O–C bonds [30]. The peak at around $1,042\text{ cm}^{-1}$ is associated with the alkoxy C–O bonds [30]. After adsorption of MB (Fig. 2(b)), the new adsorption peaks at $1,337$ and 677 cm^{-1} are clearly observed, which could be assigned to the vibration of C–N and the bending vibration of C–H in aromatic compounds, respectively [31], indicating the MB molecules have been anchored on the surface of *O. fragrans* powder. In addition, the carboxyl band at $1,630\text{ cm}^{-1}$ was shifted to $1,601\text{ cm}^{-1}$ after adsorption, suggesting a strong interaction between MB and *O. fragrans* powder [14].

3.2. Effect of adsorbent dose

The values of q_e and the removal percentage of dye ($R\%$) at different doses of *O. fragrans* powder are presented in Fig. 3. As the *O. fragrans* powders' dose is increased from 10 to 100 mg, the removal percentage of dye increases from 82.5 to 99.9%. However, the adsorption capacity (q_e) exhibits the opposite trend. The increase in the removal percentage is due to the increased adsorbent surface area and availability of more adsorption sites. The decrease in q_e is attributed to the adsorption competition among adsorbent and the split in the concentration gradient [14]. When the amount of *O. fragrans* powder was 40 mg, the $R\%$ was 98.7%. Above 40 mg of adsorbent dose, there was no significant increase in the removal rate, but q_e still decreased. Considering q_e and $R\%$, adsorbent dose of 40 mg was found to be the optimum dose for all other batch experiments.

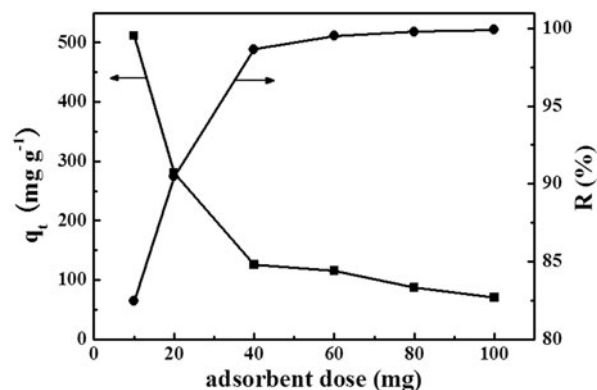


Fig. 3. Effect of adsorbent dose on the adsorption of MB ($C_0 = 70\text{ mg L}^{-1}$; initial pH 6.0; $T = 298.15\text{ K}$; $t = 160\text{ min}$).

3.3. Effect of solution pH value

The solution pH value, which can change the net charge of the adsorbent and adsorbate, is one of the most important factors in determining the adsorption properties of the adsorbent. Fig. 4 shows the effect of solution pH on MB adsorption by *O. fragrans* powder with the initial pH ranging from 2.0 to 10.0. It can be seen that the adsorption capacity of *O. fragrans* powder shows a slight increase with increasing pH value from 6.0 to 10.0. As for $\text{pH} < 6.0$, the adsorption capacity declines sharply. Accordingly, the *O. fragrans* powder exhibit a much higher adsorption capacity under neutral and alkaline conditions rather than under acidic conditions. The influence of the pH value on MB uptake could be explained on the basis of the pH_{pzc} of *O. fragrans* powder. When the pH value is

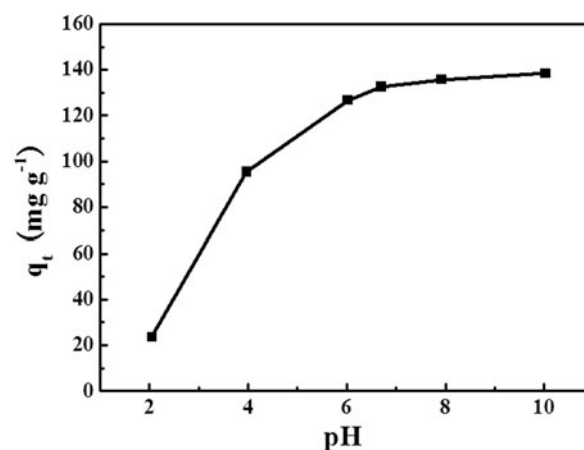


Fig. 4. Effect of solution pH on the adsorption of MB onto *O. fragrans* powder ($C_0 = 70\text{ mg L}^{-1}$; adsorbent dose = 40 mg; $T = 298.15\text{ K}$; $t = 160\text{ min}$).

lower than pH_{pzc} , it means that the surface of *O. fragrans* powder is positively charged. Otherwise, it would present a negative charge [7]. As shown in Fig. 5, the pH_{pzc} of *O. fragrans* powder is determined to be about 6.0. Therefore, the surface of *O. fragrans* powder is negatively charged under neutral and alkaline conditions, favoring the adsorption of MB in cationic form. When the pH is decreased, the adsorbent surface is more positively charged resulting in great electrostatic repulsive interactions between the *O. fragrans* powder and the MB dye. As a result, the adsorption capacity decreases obviously. By experiments, the natural pH value of suspensions was near 6.0 and it was not adjusted in other batch experiments.

3.4. Effect of salt ionic strength

It is important to discuss the effect of salt ionic strength on the adsorption of MB onto *O. fragrans* powder because industrial effluents contain not only pollutants but also high concentrations of salts, which may affect the removal of pollutants. Experiments were performed to study the effect of different sodium salts such as NaCl, Na_2SO_4 , NaNO_3 , CH_3COONa , and NaHCO_3 on MB adsorption. As shown in Fig. 6, with increasing concentrations of sodium salts, the adsorption capacities of *O. fragrans* powder decrease. Since sodium salts in MB solution can release Na^+ , the Na^+ ions may screen the electrostatic interaction of opposite charges of the adsorbent surface active sites and MB molecules; the adsorption capacities would decrease with increasing ionic strength. It is noteworthy that the different sodium salts have various effects

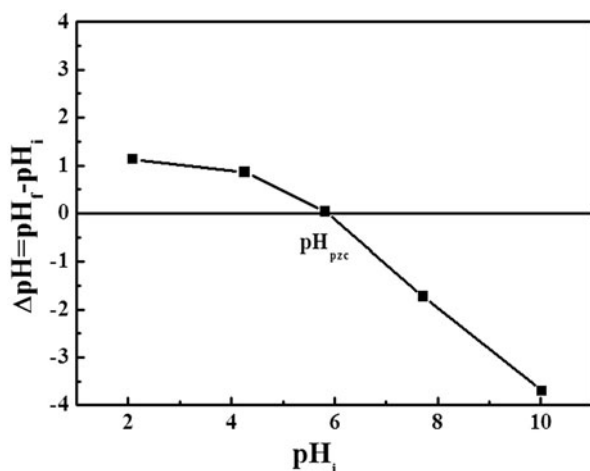


Fig. 5. The Point of zero charge (pH_{pzc}) of *O. fragrans* powder.

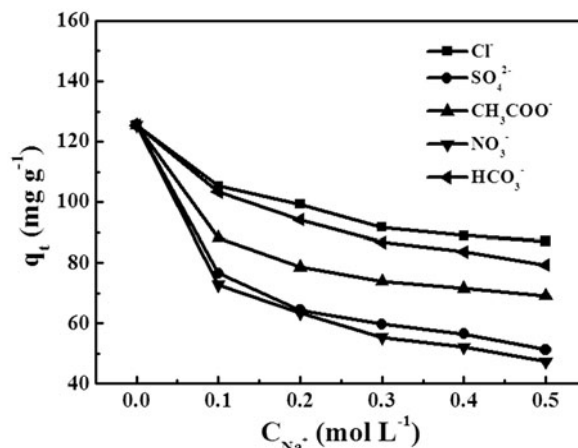


Fig. 6. Effect of different sodium salts on the adsorption of MB onto *O. fragrans* powder ($C_0 = 70 \text{ mg L}^{-1}$; adsorbent dose = 40 mg; initial pH 6.0; $T = 298.15 \text{ K}$; $t = 160 \text{ min}$).

on the adsorption performances, and the influence degree follows the order of $\text{NaNO}_3 > \text{Na}_2\text{SO}_4 > \text{CH}_3\text{COONa} > \text{NaHCO}_3 > \text{NaCl}$. This indicates that the type of anions in the solution has a remarkable effect on the adsorption capacity.

3.5. Adsorption kinetics

Fig. 7 shows the time profile of MB adsorption onto *O. fragrans* powder at different initial dye concentrations. The adsorption of MB onto *O. fragrans* powder increases with time and then attains equilibrium after 160 min. The adsorption is initially rapid, and then slows, perhaps because a large number of

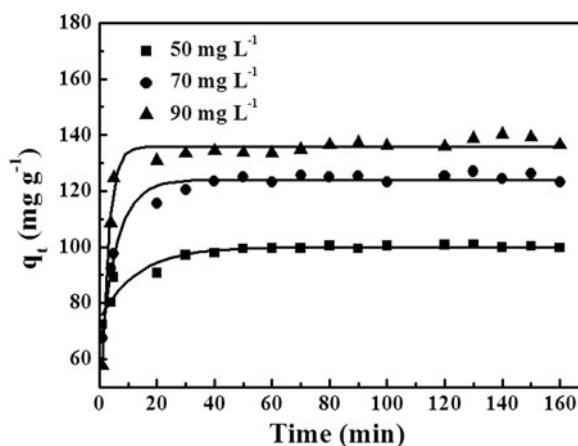


Fig. 7. Effect of contact time on the adsorption of MB onto *O. fragrans* powder at different initial dye concentrations (adsorbent dose = 40 mg; initial pH 6.0; $T = 298.15 \text{ K}$).

vacant surface sites are available for adsorption during the initial stage. And then, the remaining vacant surface sites are difficult to occupy due to the repulsive forces between the dye molecules on the *O. fragrans* powder and the aqueous phase. The adsorption capacity at equilibrium increases evidently with an increase in the initial dye concentration. This might be attributed to an increase in the driving force of concentration gradient to overcome the mass transfer resistance with an increase in the initial dye concentration [32]. To illuminate the potential application value of *O. fragrans* powder as adsorbent for the removal of MB dye from wastewater, we have compared the adsorption capacities with the commercial activated carbon. As shown in Fig. 8, the equilibrium adsorption capacity of the commercial activated carbon is about 50.61 mg g^{-1} , which is much lower than that of *O. fragrans* powder (100.85 mg g^{-1}).

To understand the characteristics of adsorption process, the kinetics of MB adsorption onto the *O. fragrans* powder is investigated using the pseudo-first-order (Fig. 9(a)) and pseudo-second-order (Fig. 9(b)) kinetic models [27,33]:

$$\log(q_e - q_t) = \log q_e - \frac{k_1}{2.303}t \quad (4)$$

$$\frac{t}{q_t} = \frac{1}{k_2 q_e^2} + \frac{1}{q_e}t \quad (5)$$

where q_e and q_t are the amounts of MB adsorbed (mg g^{-1}) at equilibrium and at time t (min), respectively, k_1 is the pseudo-first-order rate constant

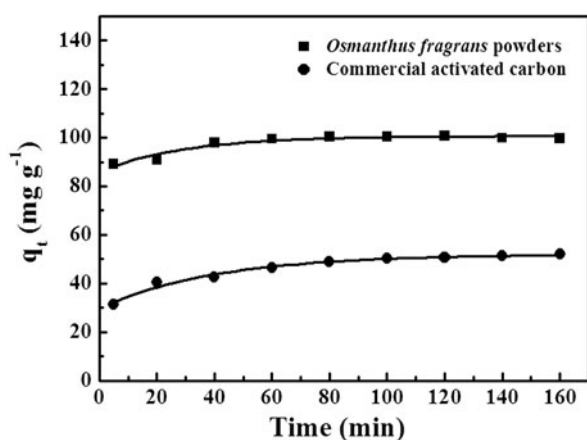


Fig. 8. Comparison of adsorption capacities of MB with commercial activated carbon ($C_0 = 50 \text{ mg L}^{-1}$; adsorbent dose = 40 mg ; initial pH 6.0; $T = 298.15 \text{ K}$).

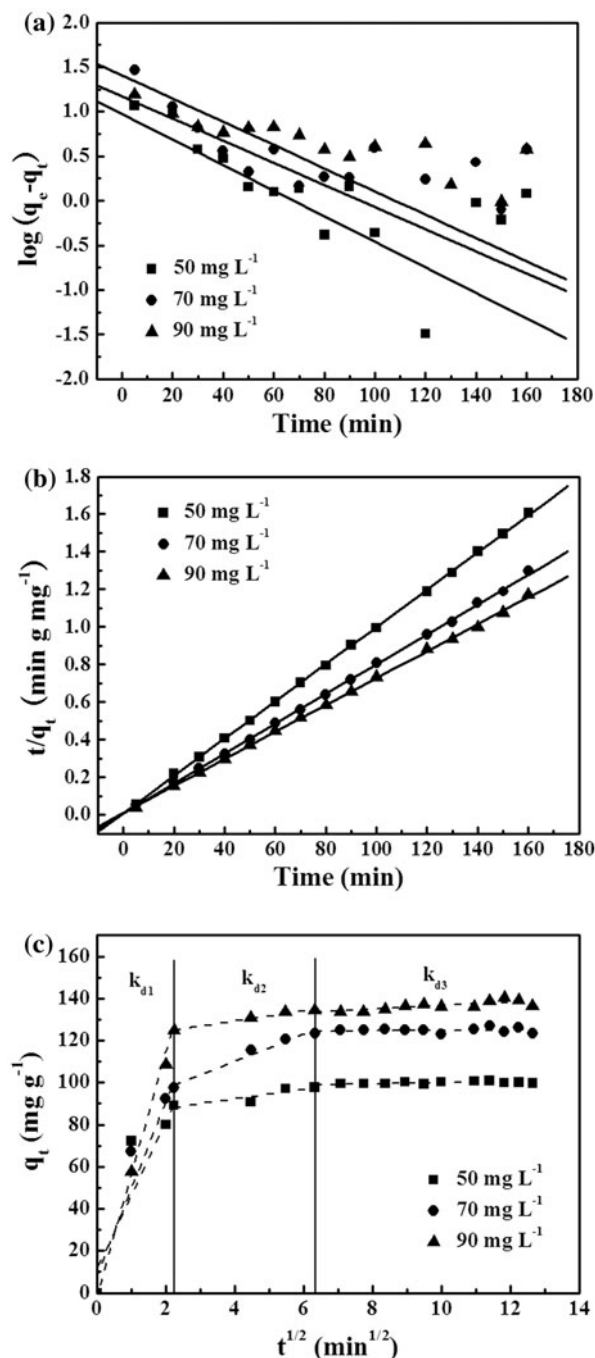


Fig. 9. Pseudo-first-order kinetics (a), pseudo-second-order kinetics (b), and intraparticle diffusion kinetics (c) plots of MB adsorption onto *O. fragrans* powder at different initial dye concentrations.

(min^{-1}), and k_2 is the pseudo-second-order rate constant (g mg min^{-1}). The conformity between experimental data and the model fitting values is expressed by correlation coefficients (R^2). As summarized in Table 1, the large differences between experimental

($q_{e,exp}$) and calculated ($q_{e,cal}$) values of the equilibrium adsorption capacity for the pseudo-first-order model indicate that the adsorption of MB onto *O. fragrans* powder does not obey the pseudo-first-order model. In contrast, the pseudo-second-order model shows a good fit with experimental data at all the studied initial concentrations ($R^2 > 0.99$). The values of $q_{e,cal}$ also exhibit to be very close to the experimental values of $q_{e,exp}$. This suggests that the pseudo-second-order model could better describe the adsorption process of MB onto *O. fragrans* powder. In addition, the pseudo-second-order rate constant (k_2) values decrease with increasing initial dye concentrations, which could be ascribed to the lower competition for the adsorption surface sites at lower concentrations [32].

Nevertheless, the above two kinetic models are not able to clarify the diffusion mechanism during the adsorption process; the intraparticle diffusion kinetic model based on the theory proposed by Weber and Morris is represented by the following equation [27,32]:

$$q_t = k_{di}t^{1/2} + C \quad (6)$$

where k_{di} is the intraparticle diffusion rate constant ($\text{mg g}^{-1} \text{min}^{-1/2}$), calculated from the slope of the straight line of q_t vs. $t^{1/2}$, C is a constant (mg g^{-1}) related to the thickness of boundary layer. A larger value of C implies the greater effect of boundary layer. Fig. 9(c) shows a linear fit of the intraparticle diffusion model at different initial dye concentrations. Three linear regions observed for all the concentrations reveal that multiple steps take place during the adsorption process of MB onto the *O. fragrans* powder. The first sharp linear section is related to the instantaneous adsorption stage that mainly occurs on the external surface of *O. fragrans* powder (film diffusion), which is completed within the first 5 min. This arises from the fact that the initial MB concentration in the solution is high and the large concentration gradient provides enough driving force for MB to diffuse into the external surface of *O. fragrans* powder. The second

adsorption region is the gradual adsorption stage corresponding to intraparticle diffusion of MB molecules through the interior pores and cavities of the adsorbent. Furthermore, the deviation of straight lines from the origin may be due to a difference in the rate of mass transfer in the initial and final stages of adsorption, indicating that the intraparticle diffusion is not the only rate-controlling step [32]. The third region is the final equilibrium stage where intraparticle diffusion further slows down owing to the low concentrations of the adsorbate left in the solutions [32]. As shown in Table 2, the k_{d1} value much greater than k_{d2} and k_{d3} suggests that the film diffusion step is an important step for the adsorption of MB onto the *O. fragrans* powder.

3.6. Adsorption isotherm

Adsorption capacities of MB onto the *O. fragrans* powder at 288.15, 298.15, and 308.15 K are illustrated by the adsorption isotherms (Fig. 10). It can be seen that the adsorption capacity of *O. fragrans* powder increases with the increasing equilibrium concentration of MB and reaches saturation progressively. The adsorption process is normally described by the Langmuir and Freundlich isotherms. The linear form of Langmuir equation can be expressed as follows [27]:

$$\frac{C_e}{q_e} = \frac{1}{q_{max}K_L} + \frac{C_e}{q_{max}} \quad (7)$$

where q_{max} is the maximum adsorption capacity of the adsorbent corresponding to a complete monolayer coverage on the surface (mg g^{-1}) and K_L is the Langmuir adsorption constant (L mg^{-1}). The constants of q_{max} and K_L can be calculated from the slope and the intercept of the linear plots of C_e/q_e vs. C_e . Fig. 11 depicts that the Langmuir adsorption isotherm fits well with experimental data. This indicates the homogeneous nature of the sample surface where each MB molecule has equal adsorption activation energy and

Table 1
Kinetic parameters for adsorption of MB onto *O. fragrans* powder

| C_0 (mg L^{-1}) | $q_{e,exp}$ (mg g^{-1}) | Pseudo-first-order | | | Pseudo-second-order | | |
|------------------------------|------------------------------------|-----------------------------|------------------------------------|--------|--|------------------------------------|--------|
| | | k_1 (min^{-1}) | $q_{e,cal}$ (mg g^{-1}) | R^2 | k_2 ($\text{g mg}^{-1} \text{min}^{-1}$) | $q_{e,cal}$ (mg g^{-1}) | R^2 |
| 50 | 100.85 | 0.0329 | 9.38 | 0.5275 | 0.0092 | 101.01 | 0.9999 |
| 70 | 126.96 | 0.0286 | 14.81 | 0.4138 | 0.0076 | 125.95 | 0.9997 |
| 90 | 140.28 | 0.0300 | 25.64 | 0.4901 | 0.0044 | 139.47 | 0.9997 |

Table 2
Intraparticle diffusion parameters for adsorption of MB onto *O. fragrans* powder

| C_0 (mg L ⁻¹) | k_{d1} (mg g ⁻¹ min ^{-1/2}) | C_1 (mg g ⁻¹) | R^2 | k_{d2} (mg g ⁻¹ min ^{-1/2}) | C_2 (mg g ⁻¹) | R^2 | k_{d3} (mg g ⁻¹ min ^{-1/2}) | C_3 (mg g ⁻¹) | R^2 |
|--------------------------------|---|--------------------------------|--------|---|--------------------------------|--------|---|--------------------------------|--------|
| 50 | 36.7756 | 12.2663 | 0.9218 | 2.2700 | 83.2055 | 0.9103 | 0.2470 | 97.4331 | 0.6393 |
| 70 | 42.3833 | 8.7992 | 0.9682 | 6.4679 | 84.2857 | 0.9863 | 0.1092 | 123.7186 | 0.1850 |
| 90 | 54.9694 | 0.8122 | 0.9995 | 2.4448 | 119.5726 | 0.9927 | 0.8323 | 128.3290 | 0.8076 |

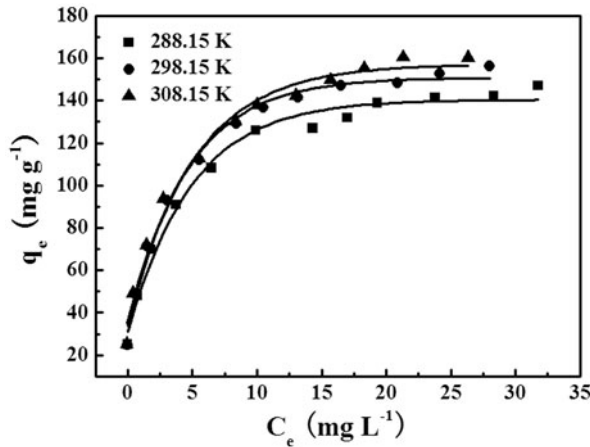


Fig. 10. Adsorption isotherms of MB on *O. fragrans* powder at different temperatures (adsorbent dose = 40 mg; initial pH 6.0; initial MB concentration = 10–90 mg L⁻¹; $t = 160$ min).

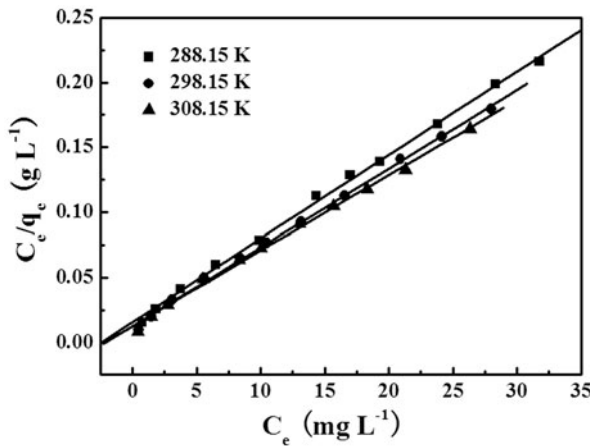


Fig. 11. Langmuir isotherm for MB adsorption onto *O. fragrans* powder at different temperatures.

demonstrates the formation of monolayer coverage of MB molecule on the surface of the adsorbent [34]. Langmuir isotherm parameters are listed in Table 3.

The essential characteristics of the Langmuir equation can be described in terms of a dimensionless

separation factor (R_L), which is defined by the following equation [34]:

$$R_L = \frac{1}{1 + K_L C_0} \tag{8}$$

where C_0 (mg L⁻¹) is the highest initial concentration of the adsorbate and K_L is the Langmuir adsorption constant (L mg⁻¹). The value of R_L indicates the type of the isotherm to be either irreversible ($R_L = 0$), favorable ($0 < R_L < 1$), linear ($R_L = 1$), or unfavorable ($R_L > 1$) [12]. Table 3 shows that the values of R_L at different temperatures are in the range of 0–1, confirming the *O. fragrans* powder are favorable for the adsorption of the MB dye.

The Freundlich adsorption isotherm describes equilibrium on heterogeneous surfaces and hence does not assume monolayer capacity. A linear form of the Freundlich model is represented by the following equation [27,34]:

$$\ln q_e = \ln K_F + \frac{1}{n} \ln C_e \tag{9}$$

where K_F (mg g⁻¹)(L mg⁻¹)^{1/n} is a rough indicator of the adsorption capacity and n is the Freundlich exponent. The values of K_F and n are calculated from the intercept and slope of the linear plots $\ln q_e$ vs. $\ln C_e$ (Fig. 12). Table 3 lists the Freundlich isotherm parameters for the adsorption of MB onto *O. fragrans* powder at 288.15, 298.15, and 308.15 K. It is clear that the values of the Freundlich exponent n are greater than 1, where $n > 1$ implies a favorable adsorption condition [34]. On the basis of a comparison of correlation coefficients R^2 values, the Langmuir isotherm model fits the adsorption data better than the Freundlich model. In other words, the adsorption of MB by *O. fragrans* powder takes place in a monolayer adsorption manner.

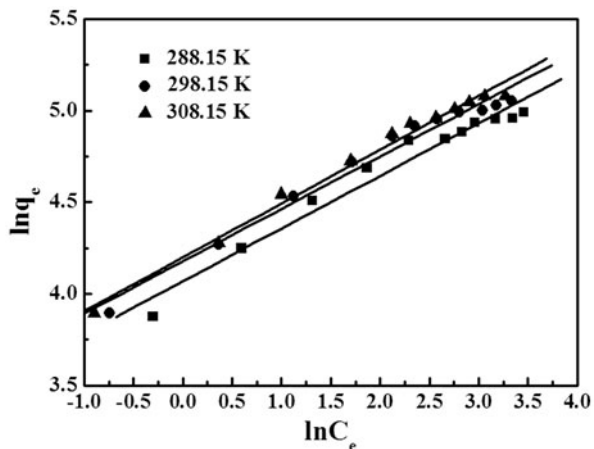
3.7. Adsorption thermodynamics

The thermodynamic parameters such as standard Gibbs free energy change (ΔG°), standard enthalpy

Table 3

Adsorption isotherm parameters for adsorption of MB onto *O. fragrans* powder

| Temperature (K) | Langmuir isotherm model | | | | Freundlich isotherm model | | |
|-----------------|----------------------------------|-----------------------------|--------|--------|---|--------|--------|
| | q_{\max} (mg g ⁻¹) | K_L (L mg ⁻¹) | R^2 | R_L | K_F (mg g ⁻¹)(L mg ⁻¹) ^{1/n} | n | R^2 |
| 288.15 | 155.52 | 0.4080 | 0.9990 | 0.0265 | 58.4967 | 3.4781 | 0.9822 |
| 298.15 | 165.02 | 0.4829 | 0.9990 | 0.0225 | 65.2568 | 3.4977 | 0.9880 |
| 308.15 | 172.71 | 0.4534 | 0.9979 | 0.0239 | 66.6750 | 3.4058 | 0.9939 |

Fig. 12. Freundlich isotherm for MB adsorption onto *O. fragrans* powder at different temperatures.

change (ΔH°), and standard entropy change (ΔS°) are determined by different temperature adsorption isotherms. The ΔG° is calculated according to following relationship [30,31]:

$$\Delta G^\circ = -RT \ln K_0 \quad (10)$$

where R is the universal gas constant (8.314 J mol⁻¹ K⁻¹), T is the Kelvin temperature, and K_0 is the adsorption equilibrium constant.

The distribution adsorption coefficient (K_d) is calculated from the following equation [30,31]:

$$K_d = \frac{C_0 - C_e}{C_e} \cdot \frac{V}{W} \quad (11)$$

where C_0 is the initial dye concentration (mg L⁻¹), C_e is the equilibrium dye concentration (mg L⁻¹), V is the volume (L) of suspension, and W is the mass of adsorbent (g). The K_0 can be obtained by plotting $\ln K_d$ vs. C_e and extrapolating C_e to zero.

The ΔH° and ΔS° are calculated from the following equation [30,31]:

$$\ln K_0 = -\frac{\Delta H^\circ}{RT} + \frac{\Delta S^\circ}{R} \quad (12)$$

The thermodynamic parameters are calculated at three different temperatures and listed in Table 4. As seen in the table, the negative ΔG° values confirm the feasibility and spontaneous nature of the adsorption process. Moreover, the value of ΔG° becomes more negative with increasing temperature, suggesting that the adsorption process of MB onto *O. fragrans* powder turns more favorable at higher temperatures. Additionally, the value of ΔG° is in the range of -20 to 0 kJ mol⁻¹, implying the adsorption process is of physisorption nature [35]. The positive ΔH° value indicates that the adsorption reaction is endothermic, which is proved by the results of adsorption capacity increasing with the enhancement of temperature (Fig. 10). The positive ΔS° value indicates the increased confusion degree during the adsorption process.

3.8. Adsorption mechanism

Five types of organic dyes such as MB, FB, RhB, OII, and MG were selected as study models to evaluate, respectively, the adsorption performances. As shown in Fig. 13, the equilibrium adsorption capacities of *O. fragrans* powder are about 119.52, 113.54, 100.85, 33.22, and 6.05 mg g⁻¹ for the MG, FB, MB, RhB, and OII, respectively. Among these dyes, the *O. fragrans* powder have relatively better adsorption performances for

Table 4

Thermodynamic parameters for adsorption of MB onto *O. fragrans* powder

| Thermodynamic constant | Temperature (K) | | |
|---|-----------------|--------|--------|
| | 288.15 | 298.15 | 308.15 |
| ΔG° (kJ mol ⁻¹) | -10.40 | -11.76 | -12.53 |
| ΔH° (kJ mol ⁻¹) | | 20.00 | |
| ΔS° (J mol ⁻¹ K ⁻¹) | | 105.82 | |

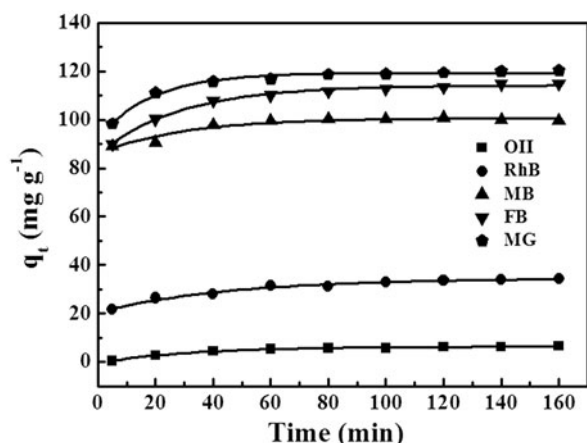


Fig. 13. Comparison of adsorption capacities of OII, RhB, MB, FB, and MG onto *O. fragrans* powder ($C_0 = 50 \text{ mg L}^{-1}$; adsorbent dose = 40 mg; initial pH 6.0; $T = 298.15 \text{ K}$).

MG, FB, and MB, moderate adsorption for RhB, and lower adsorption for OII. According to the pH_{pzc} analysis, the *O. fragrans* powder have a negative charge on its surface under the neutral and alkaline conditions. The MG, FB, MB, and RhB molecules form positively charged cations in aqueous solution and thus could be adsorbed by *O. fragrans* powder via electrostatic interaction. In contrast, OII molecules form anions in the neutral solution so they could not be largely adsorbed by *O. fragrans* powder due to the electrostatic repulsive interaction. On the other hand, although the RhB molecules form positively charged cations in solution, they have a bigger steric volume than those of MG, FB, and MB, which would restrict them to be adsorbed by *O. fragrans* powder. Therefore, the electrostatic interaction and steric hindrance effect play an important role in adsorption of dyes onto *O. fragrans* powder.

4. Conclusions

In this study, the potential of *O. fragrans* powder as a natural biosorbent was investigated for the removal of MB from aqueous solution in batch mode. The influence of experimental conditions on the adsorption performance was elucidated. The adsorption isotherm analysis showed that the Langmuir model could describe the physical adsorption process very well. The maximum adsorption capacities (q_m) of *O. fragrans* powder for MB obtained from Langmuir model were 155.52, 165.02, and 172.71 mg g^{-1} at different temperatures of 288.15, 298.15, and 308.15 K, respectively. The adsorption kinetics obeyed pseudo-second-order and intraparticle diffusion models. A

negative value of ΔG° and a positive value of ΔH° confirmed the spontaneous and endothermic nature of the adsorption process. The results indicated that *O. fragrans* powder were an effective biosorbent for the removal of MB from aqueous solution.

References

- [1] I. Ali, New generation adsorbents for water treatment, *Chem. Rev.* 112 (2012) 5073–5091.
- [2] I. Ali, M. Asim, T.A. Khan, Low cost adsorbents for the removal of organic pollutants from wastewater, *J. Environ. Manage.* 113 (2012) 170–183.
- [3] J.H. Huang, C.F. Zhou, G.M. Zeng, X. Li, J. Niu, H.J. Huang, L.J. Shi, S.B. He, Micellar-enhanced ultrafiltration of methylene blue from dye wastewater via a polysulfone hollow fiber membrane, *J. Membr. Sci.* 365 (2010) 138–144.
- [4] L.F. Albuquerque, A.A. Salgueiro, J.L. de S. Melo, O. Chiavone-Filho, Coagulation of indigo blue present in dyeing wastewater using a residual bitter, *Sep. Purif. Technol.* 104 (2013) 246–249.
- [5] O. Türgan, G. Ersöz, S. Atalay, J. Forss, U. Welander, The treatment of azo dyes found in textile industry wastewater by anaerobic biological method and chemical oxidation, *Sep. Purif. Technol.* 79 (2011) 26–33.
- [6] A.R. Khataee, M.B. Kasiri, Photocatalytic degradation of organic dyes in the presence of nanostructured titanium dioxide: Influence of the chemical structure of dyes, *J. Mol. Catal. A: Chem.* 328 (2010) 8–26.
- [7] Z.Y. Zhang, L. Moghaddam, I.M. O'Hara, W.O.S. Doherty, Congo Red adsorption by ball-milled sugarcane bagasse, *Chem. Eng. J.* 178 (2011) 122–128.
- [8] L.C. Chen, Y. Fang, Y.L. Jin, Q. Chen, Y.G. Zhao, Y. Xiao, H. Zhao, Biosorption of Cd^{2+} by untreated dried powder of duckweed *Lemna aquinoctialis*, *Desalin. Water Treat.* 53 (2015) 183–194.
- [9] B.H. Hameed, Evaluation of papaya seeds as a novel non-conventional low-cost adsorbent for removal of methylene blue, *J. Hazard. Mater.* 162 (2009) 939–944.
- [10] B.H. Hameed, M.I. El-Khaiary, Removal of basic dye from aqueous medium using a novel agricultural waste material: Pumpkin seed hull, *J. Hazard. Mater.* 155 (2008) 601–609.
- [11] V.K. Gupta, A. Nayak, Cadmium removal and recovery from aqueous solutions by novel adsorbents prepared from orange peel and Fe_2O_3 nanoparticles, *Chem. Eng. J.* 180 (2012) 81–90.
- [12] M. Achak, A. Hafidi, N. Ouazzani, S. Sayadi, L. Mandi, Low cost biosorbent “banana peel” for the removal of phenolic compounds from olive mill wastewater: Kinetic and equilibrium studies, *J. Hazard. Mater.* 166 (2009) 117–125.
- [13] E. Njikam, S. Schiewer, Optimization and kinetic modeling of cadmium desorption from citrus peels: A process for biosorbent regeneration, *J. Hazard. Mater.* 213–214 (2012) 242–248.
- [14] X.L. Han, W. Wang, X.J. Ma, Adsorption characteristics of methylene blue onto low cost biomass material lotus leaf, *Chem. Eng. J.* 171 (2011) 1–8.

- [15] S. Chakravarty, A. Mohanty, T.N. Sudha, A.K. Upadhyay, J. Konar, J.K. Sircar, A. Madhukar, K.K. Gupta, Removal of Pb(II) ions from aqueous solution by adsorption using bael leaves (*Aegle marmelos*), *J. Hazard. Mater.* 173 (2010) 502–509.
- [16] F. Deniz, S. Karaman, Removal of Basic Red 46 dye from aqueous solution by pine tree leaves, *Chem. Eng. J.* 170 (2011) 67–74.
- [17] O. Hamdaoui, F. Saoudi, M. Chiha, E. Naffrechoux, Sorption of malachite green by a novel sorbent, dead leaves of plane tree: Equilibrium and kinetic modeling, *Chem. Eng. J.* 143 (2008) 73–84.
- [18] V. Ponnusami, S.N. Srivastava, Studies on application of teak leaf powders for the removal of color from synthetic and industrial effluents, *J. Hazard. Mater.* 169 (2009) 1159–1162.
- [19] A.E. Ofomaja, E.B. Naidoo, Biosorption of copper from aqueous solution by chemically activated pine cone: A kinetic study, *Chem. Eng. J.* 175 (2011) 260–270.
- [20] F. Ferrero, Dye removal by low cost adsorbents: Hazelnut shells in comparison with wood sawdust, *J. Hazard. Mater.* 142 (2007) 144–152.
- [21] B.H. Hameed, Grass waste: A novel sorbent for the removal of basic dye from aqueous solution, *J. Hazard. Mater.* 166 (2009) 233–238.
- [22] S. Jain, R.V. Jayaram, Removal of basic dyes from aqueous solution by low-cost adsorbent: Wood apple shell (*Feronia acidissima*), *Desalination* 250 (2010) 921–927.
- [23] H. Chen, J. Zhao, G.L. Dai, Silkworm exuviae—A new non-conventional and low-cost adsorbent for removal of methylene blue from aqueous solutions, *J. Hazard. Mater.* 186 (2011) 1320–1327.
- [24] L.M. Wang, M.T. Li, W.W. Jin, S. Li, S.Q. Zhang, L.J. Yu, Variations in the components of *Osmanthus fragrans* Lour. Essential oil at different stages of flowering, *Food Chem.* 114 (2009) 233–236.
- [25] A. Kurniawan, V.O.A. Sisnandy, K. Trilestari, J. Sunarso, N. Indraswati, S. Ismadji, Performance of durian shell waste as high capacity biosorbent for Cr(VI) removal from synthetic wastewater, *Ecol. Eng.* 37 (2011) 940–947.
- [26] W. Konicki, D. Sibera, E. Mijowska, Z. Lendzion-Bieluń, U. Narkiewicz, Equilibrium and kinetic studies on acid dye Acid Red 88 adsorption by magnetic ZnFe₂O₄ spinel ferrite nanoparticles, *J. Colloid Interface Sci.* 398 (2013) 152–160.
- [27] J.B. Zhou, Z. Zhang, B. Cheng, J.G. Yu, Glycine-assisted hydrothermal synthesis and adsorption properties of crosslinked porous α -Fe₂O₃ nanomaterials for *p*-nitrophenol, *Chem. Eng. J.* 211–212 (2012) 153–160.
- [28] Y.J. Yao, B. He, F.F. Xu, X.F. Chen, Equilibrium and kinetic studies of methyl orange adsorption on multi-walled carbon nanotubes, *Chem. Eng. J.* 170 (2011) 82–89.
- [29] Y.J. Yao, S.D. Miao, S.Z. Liu, L.P. Ma, H.Q. Sun, S.B. Wang, Synthesis, characterization, and adsorption properties of magnetic Fe₃O₄@graphene nanocomposite, *Chem. Eng. J.* 184 (2012) 326–332.
- [30] J. Xu, L. Wang, Y.F. Zhu, Decontamination of bisphenol A from aqueous solution by graphene adsorption, *Langmuir* 28 (2012) 8418–8425.
- [31] J. Ma, F. Yu, L. Zhou, L. Jin, M.X. Yang, J.S. Luan, Y.H. Tang, H.B. Fan, Z.W. Yuan, J.H. Chen, Enhanced adsorptive removal of methyl orange and methylene blue from aqueous solution by alkali-activated multi-walled carbon nanotubes, *ACS Appl. Mater. Interfaces* 4 (2012) 5749–5760.
- [32] L.H. Ai, Y. Zeng, Hierarchical porous NiO architectures as highly recyclable adsorbents for effective removal of organic dye from aqueous solution, *Chem. Eng. J.* 215–216 (2013) 269–278.
- [33] Y.J. Yao, S.D. Miao, S.M. Yu, L.P. Ma, H.Q. Sun, S.B. Wang, Fabrication of Fe₃O₄/SiO₂ core/shell nanoparticles attached to graphene oxide and its use as an adsorbent, *J. Colloid Interface Sci.* 379 (2012) 20–26.
- [34] J.J. Fan, W.Q. Cai, J.G. Yu, Adsorption of N719 dye on anatase TiO₂ nanoparticles and nanosheets with exposed (001) facets: Equilibrium, kinetic, and thermodynamic studies, *Chem. Asian J.* 6 (2011) 2481–2490.
- [35] Y. Wu, H.J. Luo, H. Wang, C. Wang, J. Zhang, Z.L. Zhang, Adsorption of hexavalent chromium from aqueous solutions by graphene modified with cetyltrimethylammonium bromide, *J. Colloid Interface Sci.* 394 (2013) 183–191.